# Free-energy analysis of the nonhysteretic first-order phase transition of $Eu_2In$

B. P. Alho,[1,2,*] P. O. Ribeiro,[2,3] P. J. von Ranke,[1] F. Guillou,[4] Y. Mudryk,[2] and V. K. Pecharsky[2,5]

[1]*Instituto de Física, Universidade do Estado do Rio de Janeiro - UERJ, Rua São Francisco Xavier 524, RJ 20550-013, Brazil*

[2]*The Ames Laboratory, U.S. Department of Energy, Iowa State University, Ames, Iowa 50011-3020, USA*

[3]*Instituto de Aplicação Fernando Rodrigues da Silveira, Universidade do Estado do Rio de Janeiro - UERJ, Rua Santa Alexandrina 288, RJ 20261-232, Brazil*

[4]*Inner Mongolia Key Laboratory for Physics and Chemistry of Functional Materials, Inner Mongolia Normal University, 81 Zhaowuda Road, Hohhot 010022, Inner Mongolia, China*

[5]*Department of Materials Science and Engineering, Iowa State University, Ames, Iowa 50011-2300, USA*

(Received 15 June 2020; revised 27 August 2020; accepted 30 September 2020; published 19 October 2020)

Binary intermetallic $Eu_2In$ was recently reported to exhibit a giant anhysteretic magnetocaloric effect due to a first-order magnetic phase transition between paramagnetic and ferromagnetic states. Experimentally, the transition occurs with a small phase volume change, $\Delta V/V$, of approximately 0.1% around $T_C$ of *ca*. 55 K. We represent magnetic and compute magnetocaloric properties of a $Eu_2In$ compound using a microscopic description based on a model Hamiltonian that takes into account magnetic exchange and magnetoelastic interactions. In the model the thermodynamic nature of the transition is conveniently represented by a single magnetoelastic interaction parameter. A good agreement between the theoretical results and earlier published experimental data confirms the effectiveness of our approach.

DOI: 10.1103/PhysRevB.102.134425

## I. INTRODUCTION

Reversible thermal phenomena observed in materials during the application and removal of an external magnetic field, known as the magnetocaloric effect (MCE), are of both fundamental and practical significance. The effect is usually quantified by two thermodynamic functions, namely, the isothermal entropy change $\Delta S_T$ and the adiabatic temperature change $\Delta T_{ad}$ [1,2]. Basic and applied research focused on compounds exhibiting strong MCEs has greatly increased over the last two decades due to their potential to support future applications in near-room-temperature magnetocaloric heat pumping [3–5]. In addition to the near-room-temperature region, magnetocaloric refrigeration is a promising approach for a cryogenic regime, for example, energy-efficient liquefaction of gases, including hydrogen [6].

For a compound to be useful in the realm of magnetocaloric cooling, the material must demonstrate high absolute values of both $\Delta S_T$ and $\Delta T_{ad}$ with negligible hysteresis in response to manageable magnetic field changes. Added to these critical performance parameters, practical magnetocaloric refrigerants must also be chemically and mechanically stable, nontoxic, and affordable. Strong magnetocaloric effects are generally achieved through first-order magnetic phase transformations (FOMTs), which can lead to $|\Delta S_T|$ and $|\Delta T_{ad}|$ much greater than those observed during second-order magnetic phase transitions, and these large MCEs are commonly known as the giant magnetocaloric effects (GMCEs) [7,8]. The majority of FOMTs, however, are associated with thermal and magnetic hystereses, as is the case for the prototypical compounds exhibiting GMCE, such as $Gd_5(Ge_{1-x}Si_x)_4$, $La(Fe_{1-x}Si_x)_{13}$, and its derivatives and hydrides, FeRh, and $(Mn, Fe)_2(P, As, Si)$ [9–16]. While it is rather difficult to realize GMCE with almost no hysteresis, such a combination has been achieved in some materials systems by compositional doping, for example, in MnFe(P,Si,B) [17].

As follows from published literature, only a few compounds exhibit clearly discontinuous FOMTs with negligible or no intrinsic hysteresis. Among those, a high-purity Dy metal shows a nearly ideal FOMT between antiferromagnetic (AFM) and ferromagnetic (FM) phases, which also involves an orthorhombic distortion of the hcp structure of the metal stable in both the paramagnetic (PM) and AFM states [18]. Other examples include nonhysteretic FOMTs at the spontaneous spin reorientation transition in $HoAl_2$ [19–21], at the long-range magnetic ordering transition of $DyCo_2$ accompanied by cubic-tetragonal distortion and minor discontinuities of unit-cell dimensions and phase volume [7], and more recently, magnetoelastic transformations in $R_2In$ compounds when $R =$ Eu or Pr [22,23]. In the binary $Eu_2In$ intermetallic compound, the filling of the Eu $5d$ states due to hybridization with Eu $6s$, $6p$, and In $5p$ states has been identified as the main electronic mechanism for the emergence of an FOMT. Crystallographic symmetry across the FOMT in $Eu_2In$ remains unperturbed, hence the transition is isostructural, and it is accompanied by a very small volume discontinuity, $\Delta V/V$, on the order of 0.1%. This similarity between the crystallographic lattices in both the PM and FM states of $Eu_2In$ is

*Corresponding author: B. P. Alho, Universidade do Estado do Rio de Janeiro, IF - DEQ Rua São Francisco Xavier, 524 - 3$^0$ andar. Maracanã, Rio de Janeiro - 20550-013, Brazil; brunoalho@gmail.com

 

an important factor leading to low-strain energy barriers and miniscule hysteresis.

In agreement with the band structure described in [22], a purely electronic mechanism associating the anhysteretic behavior of $Eu_2In$ with Fermi-surface topology changes triggered by spin polarization has been recently proposed [24]. Here we investigate the anhysteretic character of the FOMT in $Eu_2In$ through the analysis of the magnetic free-energy landscape derived using a model Hamiltonian that takes into account magnetic exchange and magnetoelastic interactions. In this phenomenological model, which is nonselective with respect to the details of the electronic structure, the underlying modifications that occur at the level of electrons are incorporated as changes in the exchange interactions between the localized $4f$ electrons of Eu included in the Hamiltonian through the magnetoelastic interaction. The magnetic field dependences of the Curie temperature, magnetization, and magnetocaloric effect vs temperature predicted by our model are in good agreement with experimental data, confirming that such an approach complements results derived *ab initio* and can be useful in the future for both rationalizing experimental results and guiding the design of materials exhibiting GMCE without unfavorable hysteresis.

## II. THEORY

In order to describe the FOMT in $Eu_2In$, we consider a model Hamiltonian in the mean-field approximation [25,26] that includes exchange and magnetoelastic interactions:

$$\hat{\mathcal{H}} = -g\mu_B(\lambda M + DM^3 + \mu_0 H)J^z, \tag{1}$$

where $\lambda = 2z\gamma/Ng^2\mu_B^2$ is the exchange parameter, which can also be written as $\lambda = \frac{3k_BT_0}{g^2\mu_B{}^2J(J+1)}$, where $T_0$ is the Curie temperature of a standard second-order ferromagnetic-paramagnetic phase transition in the absence of magnetoelastic interactions; $D = 4z\zeta/N^3g^4\mu_B^4$ is the measure of the magnetoelastic interactions, which as explained below, is also used to adjust the thermodynamic nature of the phase transition at $T_C$ within the model; $z$ is the number of the nearest-neighbor atoms; $N$ is the number of magnetic ions per unit cell; $\gamma$ and $\zeta$ are the exchange and magnetoelastic energies, respectively; $M = Ng\mu_B\langle J^z\rangle$ is the magnetization; $g$ is the Landè factor; $\mu_B$ is the Bohr magneton; and $\mu_0 H$ is the applied magnetic field. The magnetoelastic parameter, $D$, is introduced into the model to account for variability of exchange interactions with interatomic distances at $\lambda = const$. Increasing $D$ beyond a certain critical value $D_C$ at fixed $\lambda$ leads to a higher magnetic transition temperature $T_C$; hence in the model $T_C$ becomes dependent on both $D$ and $\lambda$. We note that for a given $\lambda$ when $D < D_C$ the transition at $T_C$ is second order, and it becomes first order when $D > D_C$ [26–28]. The associated phase volume change is included in the model through a change in the Debye temperature $\theta_D$:

$$\theta_D = \theta_0(1 - \Gamma\omega), \tag{2}$$

where $\theta_0$ is the Debye temperature without the relative volume change, $\omega$ is the relative volume change, and $\Gamma$ is the Grüneisen parameter [29,30]. When including the magnetoelastic coupling in the lattice entropy, the relative volume change is considered proportional to the magnetization squared [30–34], and relation (2) can be rewritten, in terms of the normalized Grüneisen parameter $\Gamma^D$, as

$$\theta_D = \theta_0(1 - \Gamma^D M^2). \tag{3}$$

By obtaining the eigenvalues from the Hamiltonian (1), one may calculate the partition function $Z$ and the magnetic free energy $\Phi$, including the magnetic work as described in Ref. [26] and given by

$$\Phi = -k_BT\ln[Z] + \frac{\lambda M^2}{2} + \frac{3DM^4}{4} + k_BT\ln[Z_0], \tag{4}$$

where $k_B$ is the Boltzmann constant and $Z_0$ is the partition function for zero magnetization. For a given set of model parameters, the magnetization can be determined by minimizing the magnetic free energy. Neglecting the electronic entropy (see below), the total entropy of a system ($S_T$) includes the magnetic ($S_{\text{mag}}$) and lattice ($S_{\text{latt}}$) entropies and is given by

$$S_T(T, \mu_0 H) = S_{\text{mag}}(T, \mu_0 H) + S_{\text{latt}}(T, \mu_0 H), \tag{5}$$

where $S_{\text{mag}}$ is the usual mean-field magnetic entropy and $S_{\text{latt}}$ is given by the Debye approximation [35], written as follows:

$$S_{\text{latt}}(T, \mu_0 H) = N_A\mathcal{R}\left[-3\ln\left(1 - e^{-\frac{\theta_D}{T}}\right) + 12\left(\frac{T}{\theta_D}\right)^3\int_0^{\frac{\theta_D}{T}}\frac{y^3}{e^y - 1}dy\right], \tag{6}$$

where $N_A = 3$ is the number of atoms per formula unit, and $\mathcal{R}$ is the universal gas constant. It is worth noting that $S_{\text{latt}}$ is magnetic field dependent, since the magnetic field induces the transition between the PM and FM states that have slightly different phase volumes, and in our model the Debye temperature also depends on the magnetization. The isothermal entropy change is computed as

$$\Delta S_T(T, \mu_0\Delta H) = S_T(T, \mu_0 H_2) - S_T(T, \mu_0 H_1), \tag{7}$$

with $H_2 > H_1$. While the lattice entropy must be included in the $\Delta S_T$ calculation, we assume that the electronic contribution to the total entropy ($S_{\text{el}} = \gamma_{\text{el}}T$, where $\gamma_{\text{el}}$ is the Sommerfeld coefficient) only depends on temperature and thus does not contribute to $\Delta S_T$ values. The adiabatic temperature change can be directly calculated from a pair of total entropy curves $S_T(T, \mu_0 H_2)$ and $S_T(T, \mu_0 H_1)$ in the adiabatic process when $S_T(T, \mu_0 H_1) = S_T(T, \mu_0 H_2)$ and is given by

$$\Delta T_{\text{ad}}(T, \mu_0\Delta H) = T_2(T, \mu_0 H_2) - T_1(T, \mu_0 H_1). \tag{8}$$

## III. RESULTS AND DISCUSSIONS

As mentioned above, for a given set of model parameters ($T_0$, $D$) the magnetic phase transition may be of second ($D < D_C$) or first order ($D > D_C$). The order of the phase transition is determined by analyzing the first derivative of the magnetic free energy [relation (4)] with respect to magnetization for the presence of mathematical critical points (MCPs), defined as $\partial\Phi/\partial M = 0$. If the phase transition is of second (first) order, $\Phi$ may exhibit at most three (five) MCPs, respectively. Through analysis of temperature and magnetic field

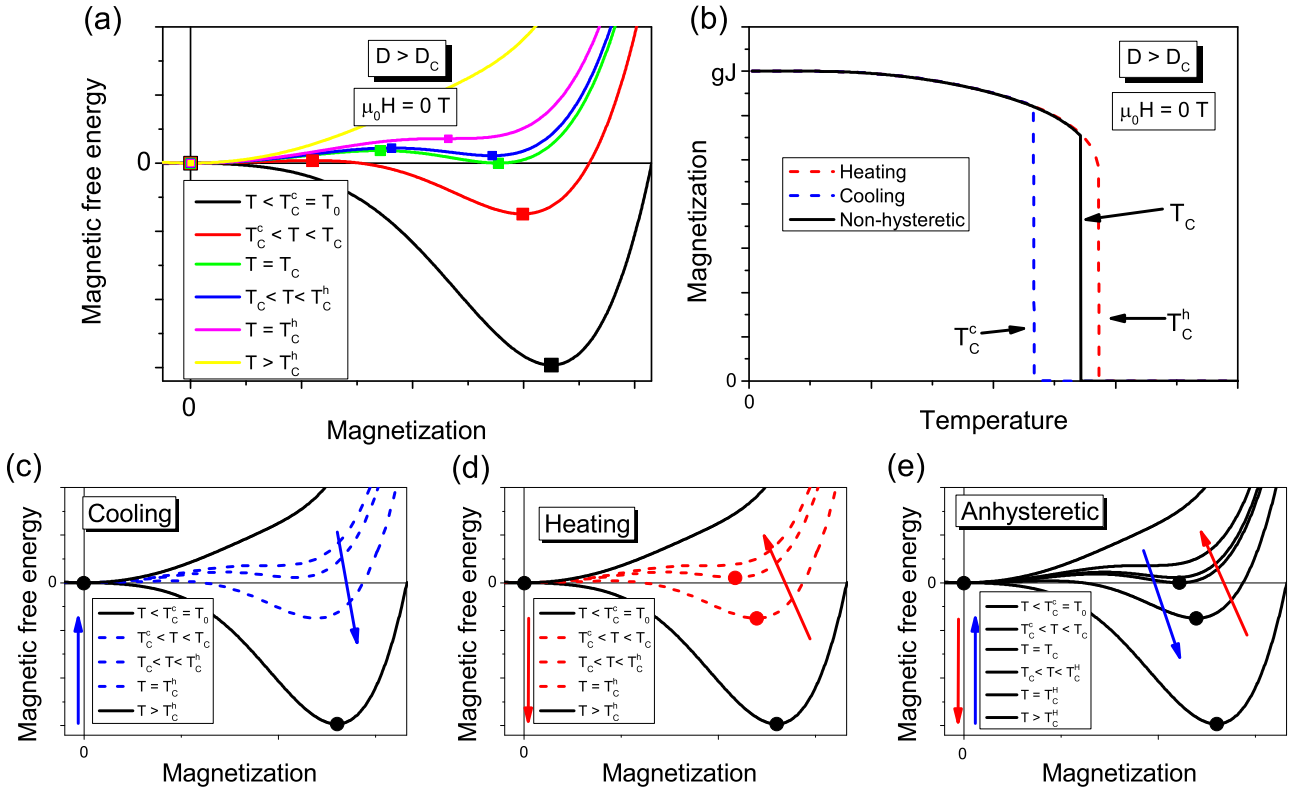


FIG. 1. (a) Schematic representation of the magnetic free energy vs spontaneous magnetization at selected temperature regions, namely, $T < T_C^c$ (black), $T_C^c < T < T_C$ (red), $T = T_C$ (green), $T_C < T < T_C^h$ (blue), $T = T_C^h$ (magenta), and $T > T_C^h$ (yellow). Symbols represent the mathematical critical points defined as $\partial\Phi/\partial M = 0$. (b) Schematic spontaneous magnetization vs temperature dependence for the nonhysteretic (black curve) and hysteretic first-order phase transformations. For the latter, the heating part is presented by a red dashed curve and cooling part by a blue dashed curve. (c) Magnetic free-energy scheme for the cooling process for the hysteretic scenario. Blue arrow represents the decreasing temperature. The black circles mark the minimum energy path. (d) Magnetic free-energy scheme for the heating process for the hysteretic scenario. Red arrow represents the increasing temperature. The black and red circles mark the minimum energy path. (e) Magnetic free-energy scheme for the anhysteretic scenario. Blue and red arrows represent decreasing and increasing temperatures, respectively. The black circles mark the minimum energy path.

dependence of the MCPs the minimum energy path may be evaluated, which gives rise to thermal and magnetic hysteresis due to metastable states present in the magnetic free-energy landscape.

Figure 1(a) shows a general scheme of the magnetic free energy as function of magnetization with the MCPs marked with symbols. There are two extreme cases that we describe in more detail. In the first case (for example, MnAs [26]), the system is trapped in a local free-energy minimum, due to large energy barriers, and can only change state when both the minimum and the associated energy barrier disappear as temperature and/or magnetic field vary, resulting in large thermal and/or magnetic hystereses. This can be seen in Fig. 1(d), where starting from a minimum with $M > 0$ in the magnetically ordered state, the transition on heating occurs spontaneously at a certain $T_C^h > T_C$ when the minimum disappears and magnetization is abruptly reduced to 0. The corresponding $M(T)$ is shown in Fig. 1(b) as the red dashed line. Conversely, starting from a global minimum with $M = 0$ in the paramagnetic state, the transition occurs at $T_C^c < T_C$, with $T_C^c = T_0$, when the free energy evolves such that the minimum becomes a maximum at $M = 0$, and the system changes state by moving without an energy barrier into another minimum that develops at $M > 0$, as can be seen in Fig. 1(c). The magnetization as a function of temperature upon cooling is illustrated in Fig. 1(b) with the blue dashed line.

The second scenario leads to anhysteretic behavior, and it occurs when energy barriers (e.g., due to strain) are negligibly small. Then the system can easily follow the free-energy global minimum path between $M = 0$ and $M > 0$ states. In Fig. 1(e), the transition occurs at $T_C$ for both heating and cooling, and the corresponding behavior of magnetization is shown in Fig. 1(b) with the black solid line. Since the FOMT in $Eu_2In$ occurs without a change of crystallographic symmetry and with very small discontinuity in phase volume, it is reasonable to assume that in the title material the energy required to overcome the strain energy barrier(s) does not exceed $k_B T_C$, leading to an anhysteretic transition [22]. We note that the electronic mechanism of Ref. [24] describing the anhysteretic behavior of $Eu_2In$ confirms this scenario as well. Here, the Fermi energy $E_F$ is located near the top of Eu $5d$ and In $5p$ bands, which plays an important role in determining how interactions between the localized $Eu^{2+}$ $4f$ moments are mediated by the hybridized Eu $5d$ and In $5p$ states [24]. When $E_F$ is located near the top or the bottom of a band, the density of states at $E_F$ becomes strongly dependent on magnetic moments, and this dependence strengthens (or weakens) the indirect magnetic exchange interactions, thus

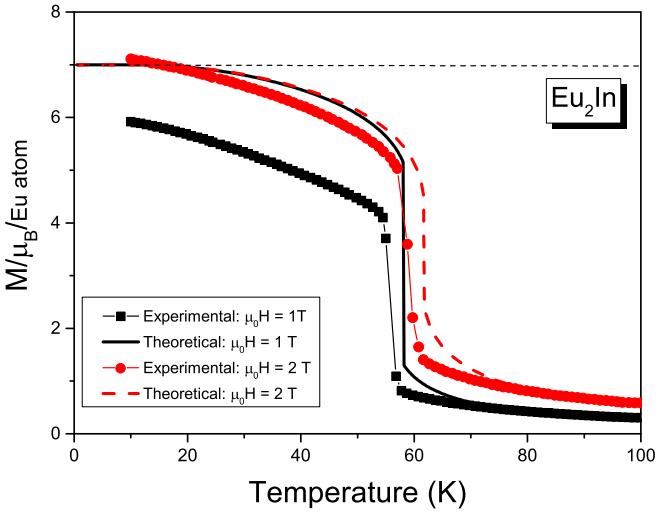


FIG. 2. Magnetization of $Eu_2In$ measured experimentally (symbols, from Ref. [22]) and predicted from the model (lines) in 1- (black) and 2-T (red) magnetic fields.

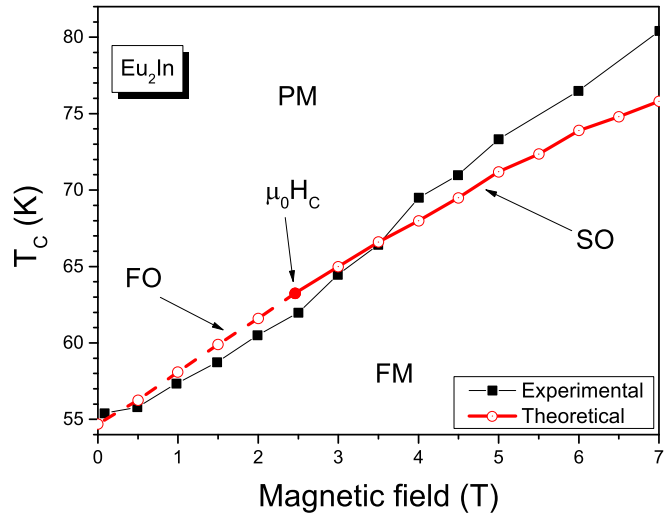


FIG. 3. *H-T* phase diagram of $Eu_2In$. Experimental data of Ref. [22] are shown using closed squares and the theoretical results are shown using open circles. The full circle represents the theoretically predicted $\mu_0 H_C$, above which the magnetovolume transition is second order, also depicted by the solid line, and the magnetovolume phase transition is first order when $\mu_0 H < \mu_0 H_C$, as shown by the dashed line.

driving the FM↔PM transition in $Eu_2In$ without hysteresis [24]. The changes in the Eu $4f$ exchange interactions derived explicitly from first principles in [24] are included implicitly in our phenomenological model through the magnetoelastic parameter.

We note that the scenarios mentioned above represent two extreme cases, and a rigorous definition of the energy barrier without clear assumptions makes proper constraining of the microscopic Hamiltonian challenging [35–38]. In $Eu_2In$, experimental data indicate the absence of hysteresis, thus pointing to the nearly negligible energy barrier when compared to $k_B T$, as described above and depicted schematically in Fig. 1(e). Hence a simple treatment of hysteresis by only considering the magnetic free energy appears to be sufficient for modeling of the phase transformation in $Eu_2In$.

The following model parameters for $Eu_2In$ compound were determined by fitting the experimental data, i.e., the temperature dependencies of magnetization and $-\Delta S_T$ reported in Ref. [22]: $T_0 = 46$ K, $D = 500\,\mathrm{T}^4/\mathrm{meV}^3$, $\Gamma^D = -1.5\,\mathrm{T}^2/\mathrm{meV}^2$, and $\theta_0 = 250$ K. In line with a minor phase volume change observed in $Eu_2In$, the value of the magnetoelastic parameter is much smaller when compared with results reported for other compounds, such as MnAs ($D \sim 21\,000\,\mathrm{T}^4/\mathrm{meV}^3$) [26] and $Gd_5Si_2Ge_2$ ($D \sim 1500\,\mathrm{T}^4/\mathrm{meV}^3$) [33]. Figure 2 shows the temperature dependence of the magnetization for $Eu_2In$ in applied magnetic fields of 1 and 2 T, where the symbols and lines represent experimental data of Ref. [22] and modeling results, respectively. Minimization of the magnetic free energy [relation (4)] following the global minima path gives the magnetization values presented in Fig. 2. The theoretical results reproduce a saturation magnetization at $gJ = 7\,\mu_B$/Eu atom for both magnetic fields; hence the magnetization values for $\mu_0 H = 1$ T are overestimated by the model since this field strength is not sufficient to saturate the compound's magnetization. For a 2-T magnetic field, the experimental data saturate slightly above $7\,\mu_B$/Eu atom due to contributions from the $5d$ electrons [22].

Figure 3 depicts the *H-T* phase diagram comparing theoretical predictions with experimental results for the magnetic field dependence of the transition temperature ($T_C$). The two sets of data are in good agreement for magnetic fields up to 5 T. In addition to reproducing field-dependent transformation temperatures at $T_C$, our theoretical model enables one to estimate a critical magnetic field at which the order of the magnetovolume phase transition in $Eu_2In$ changes from the first order to the second order. This is possible by examining how the number of MCPs in the magnetic free energy as a function of magnetization changes with respect to temperature and applied magnetic field. Such a theoretical prediction of the critical magnetic field required to change the order of phase transition is of importance, since experimentally distinguishing a broadened FOMT from a second-order transition is not straightforward. The model predicts a critical magnetic field of $\mu_0 H_c \sim 2.46$ T (shown as the filled circle in Fig. 3), i.e., when $\mu_0 H > \mu_0 H_c$(solid line) the magnetovolume transition in $Eu_2In$ thermodynamically becomes second order, and the first-order nature of this transition (dashed line in Fig. 3) is retained when $\mu_0 H < \mu_0 H_c$. The existence of an earlier indistinguishable critical point is commensurate with the reported experimental data, which show a significant broadening of the heat capacity peak already occurring in a 2-T magnetic field [22]. In this regard, the behavior of the title material is similar to that earlier reported in $DyCo_2$ [7], where a magnetic field of 4 T completely suppresses phase volume discontinuity and makes it a continuous change that occurs over some 30-K interval, converting the first-order magnetostructural phase transition at low magnetic fields into the second-order magnetostructural transformation at high magnetic fields. Notably, the transformation in $DyCo_2$ is anhysteretic as well.

The temperature dependence of the isothermal entropy change is shown in Fig. 4. Similar to $M(T)$, there is a

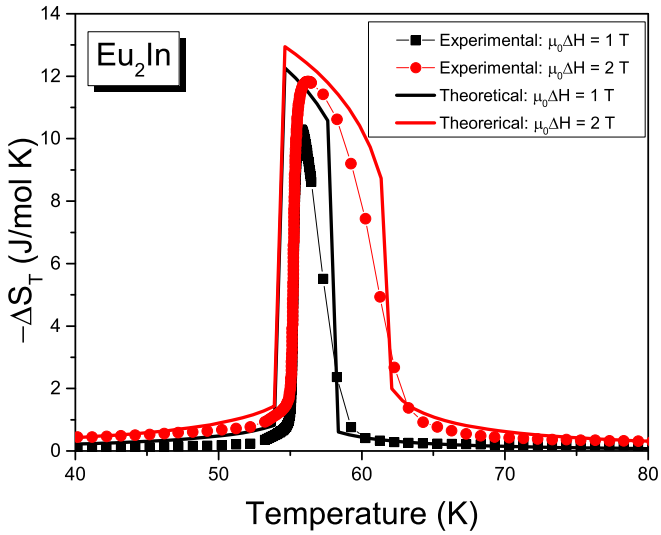


FIG. 4. Isothermal entropy change $(-\Delta S_T)$ vs temperature for the $Eu_2In$ compound for 0–1 T (black curves) and 0–2 T (red curves) magnetic field changes. Closed symbols are the experimental data [22], and solid lines the theoretical results.

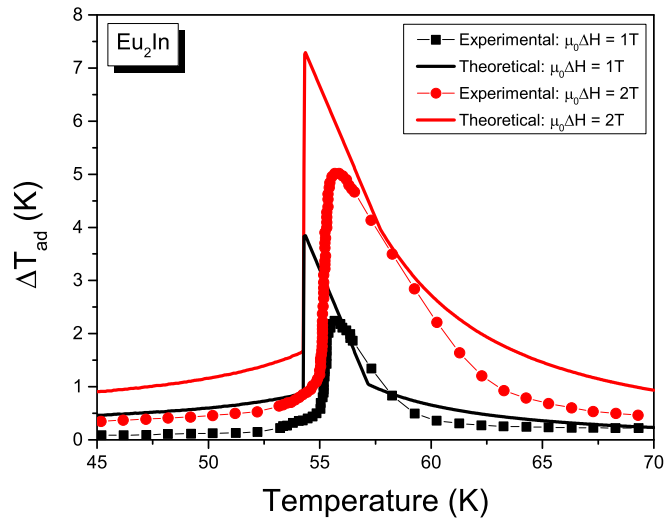


FIG. 5. Adiabatic temperature change $(\Delta T_{ad})$ vs temperature in $Eu_2In$ compound for 0–1 T (black curves) and 0–2 T (red curves) magnetic field changes. Closed symbols are the experimental data [22], and solid lines the theoretical results.

good agreement between the theoretical predictions and the experimental data of Ref. [22]. The main discrepancies are due to a truly discontinuous character of the FOMT imposed by the model, while experimentally the magnetocaloric effect rises and falls not as sharply due to the finite width of the transition observed in a real material, which also includes a narrow phase-separated region. We note that in the model we consider coupling between the magnetism and the lattice through relation (3). Therefore our theoretical $\Delta S_T$ includes both the magnetic and lattice entropy changes, and one can estimate their respective contributions to the total entropy change. At the MCE peak temperature, which coincides with $T_C = 54.6\,\mathrm{K}$, the magnetic and lattice contributions respectively account for ∼70% and ∼30% of the total. As already mentioned above, the electronic entropy does not contribute to $\Delta S_T$ since it is considered independent of the magnetic field, i.e., $S_{el}(T, H)_H = const$.

The temperature dependence of $\Delta T_{ad}$ illustrated in Fig. 5 was calculated using relation (8), including the electronic contribution in the total entropy. In order to include the electronic entropy contribution in $S_T$ we use the Sommerfeld's approximation ($S_{el} = \gamma_{el} T$), where $\gamma_{el}$ is the Sommerfeld coefficient. In our simulations we adopt $\gamma_{el} = 0.0054\,\mathrm{J/mol\,K^2}$, the value obtained for $RAl_2$ compounds [39,40], which is nearly identical to $\gamma_{el} = 0.005\,\mathrm{J/mol\,K^2}$ of $Yb_2In$ determined from the low-temperature heat capacity of the closely related compound isostructural with $Eu_2In$ (our unpublished data). We note that magnetic contributions to the specific heat of $Eu_2In$ are non-negligible down to the lowest temperature of the measurements reported in Ref. [22], thus precluding direct determination of $\gamma_{el}(Eu_2In)$. For the temperature range of interest in $Eu_2In$, the electronic contribution in $S_T$, and therefore in $\Delta T_{ad}$, is negligible, even for the Sommerfeld's coefficient one order of magnitude higher.

The shapes of the $\Delta T_{ad}(T)$ agree well, even though theoretical values are higher than the experimental results. The theoretical peak values of $\Delta T_{ad}$ are around 3.8 and 7.2 K for magnetic field changes of 1 and 2 T, respectively. When compared with the experimental data they are 70% and 40% higher, in that order. Once again, these discrepancies can be ascribed to the truly discontinuous character of the phase transition in the model, which leads to greater isentropic differences evaluated using relation (8) when compared to the isothermal separation between the two entropy curves represented by relation (7). Our theoretical model also predicts that the lattice contribution to the adiabatic temperature change due to magnetoelastic coupling, which is around a third of the total $\Delta T_{ad}$ just below $T_C$ in a zero magnetic field, e.g., for $T = 53\,\mathrm{K}$, becomes nearly negligible at the peak value ($T = 54.4\,\mathrm{K}$). The latter is also due to the discontinuous character of the magnetic phase transition in our model. For a first-order transition, the effect of the applied magnetic field is to shift the entropy discontinuity to higher temperatures, and hence the peak value of the adiabatic temperature change can be approximated as $\Delta T_{peak} \sim T_C(\mu_0 H \neq 0) - T_C(\mu_0 H = 0)$ [41]. As a result, the $\Delta T_{peak}$ only depends on how rapidly the magnetic field shifts the transition temperature and is only weakly dependent on the lattice contributions to $\Delta S_T$.

## IV. CONCLUSIONS

Magnetic and magnetocaloric properties of $Eu_2In$ were investigated using a model that includes the exchange and magnetoelastic interactions in the mean-field approximation. The coupling between the magnetic and lattice entropies was treated using the Grüneisen assumption of the Debye temperature dependence on lattice deformation. We identify a previously unknown critical magnetic field above which the first-order magnetovolume transformation in $Eu_2In$ is projected to become second order. We also demonstrate that anhysteretic behavior of magnetization across the

magnetovolume transition in $Eu_2In$ can be explained considering the evolution of the magnetic free energy as a function of magnetization with temperature. In addition to a good agreement between the modeling results and the experimental data, we show that despite a rather small phase volume change, lattice distortion accounts for about a third of the magnetic-field-induced entropy change, $\Delta S_T$, of $Eu_2In$. Maximum adiabatic temperature change, $\Delta T_{ad}$, on the other hand, is not enhanced by the accompanying phase volume change. The proposed model is an important step toward a better physical description of the magnetovolume transformation in the title compound, and it could be applied to other compounds, which present similar transitions with or without hysteresis.

## ACKNOWLEDGMENTS

The Ames Laboratory is operated for the U. S. Department of Energy (DOE) by Iowa State University of Science and Technology under Contract No. DE-AC02-07CH11358. This work was supported by the Office of Science of the U.S. DOE, Division of Materials Sciences and Engineering, Office of Basic Energy Sciences. Two of us (P.O.R. and B.P.A.) acknowledge financial support from Coordenação de Aperfeiçoamento de Pessoal de Nível Superior - Brasil (CAPES) - Finance Code 001, CNPq - Conselho Nacional de Desenvolvimento Científico e Tecnológico - Brazil, FAPERJ - Fundação de Amparo à Pesquisa do Estado do Rio de Janeiro.

[1] K. A. Gschneidner Jr. and V. K. Pecharsky, Rep. Prog. Phys. **68**, 1479 (2005).
[2] V. Franco, J. S. Blázquez, J. J. Ipus, J. Y. Law, L. M. Moreno-Ramírez, and A. Conde, Prog. Mater. Sci. **93**, 112 (2018).
[3] V. K. Pecharsky and K. A. Gschneidner Jr., J. Magn. Magn. Mater. **200**, 44 (1999).
[4] O. Gutfleisch, M. A. Willard, E. Brück, C. H. Chen, S. G. Sancar, and J. P. Liu, Adv. Mater. **23**, 821 (2011).
[5] A. Smith, Adv. Energy Mater. **2**, 1288 (2012).
[6] T. Numazawa, K. Kamiya, T. Utaki, and K. Matsumot, Cryogenics **62**, 185 (2014).
[7] V. K. Pecharsky, K. A. Gschneidner Jr., Y. Mudryk, and D. Paudyal, J. Magn. Magn. Mater. **321**, 3541 (2009).
[8] K. A. Gschneidner Jr., Y. Mudryk, and V. K. Pecharsky, Scr. Mater. **67**, 572 (2012).
[9] V. K. Pecharsky and K. A. Gschneidner Jr., Phys. Rev. Lett. **78**, 4494 (1997).
[10] O. Tegus, E. Brück, K. H. J. Buschow, and F. R. de Boer, Nature (London) **415**, 150 (2002).
[11] H. Wada and Y. Tanabe, Appl. Phys. Lett. **79**, 3302 (2001).
[12] F. X. Hu, B. G. Shen, J. R. Sun, Z. H. Cheng, G. H. Rao, and X. X. Zhang, Appl. Phys. Lett. **78**, 3675 (2001).
[13] S. Gama, A. A. Coelho, A. de Campos, A. M. G. Carvalho, F. C. G. Gandra, P. J. von Ranke, and N. A. de Oliveira, Phys. Rev. Lett. **93**, 237202 (2004).
[14] A. Campos, D. L. Rocco, A. M. G. Carvalho, L. Caron, A. A. Coelho, S. Gama, L. M. Silva, F. C. G. Gandra, A. O. Santos, P. J. von Ranke, and N. A. de Oliveira, Nat. Mater. **5**, 802 (2006).
[15] M. P. Annaorazov, S. A. Nikitin, A. L. Tyurin, K. A. Asatryan, and A. Kh. Dovletov, J. Appl. Phys. **79**, 1689 (1996).
[16] A. Chirkova, K. P. Skokov, L. Schultz, N. V. Baranov, O. Gutfleisch, and T. G. Woodcock, Acta Mater. **106**, 15 (2016).
[17] F. Guillou, G. Porcari, H. Yibole, N. van Dijk, and E. Brück, Adv. Mater. **26**, 2671 (2014).
[18] V. K. Pecharsky, K. A. Gschneidner Jr., and D. Fort, Scr. Mater. **35**, 843 (1996).
[19] B. Barbara, M. F. Rossignol, and J. X. Boucherle, Phys. Lett. A **55**, 321 (1975).
[20] V. S. R. de Sousa, L. E. L. Silva, A. M. Gomes, and P. J. von Ranke, J. Alloys Compd. **686**, 522 (2016).
[21] M. Khan, K. A. Gschneidner Jr., and V. K. Pecharsky, J. Appl. Phys. **110**, 103912 (2011).
[22] F. Guillou, A. K. Pathak, D. Paudyal, Y. Mudryk, F. Wilhelm, A. Rogalev, and V. K. Pecharsky, Nat. Commun. **9**, 2925 (2018).
[23] A. Biswas, N. A. Zarkevich, A. K. Pathak, O. Dolotko, I. Z. Hlova, A. V. Smirnov, Y. Mudryk, D. D. Johnson, and V. K. Pecharsky, Phys. Rev. B **101**, 224402 (2020).
[24] E. Mendive-Tapia, D. Paudyal, L. Petit, and J. B. Staunton, Phys. Rev. B **101**, 174437 (2020).
[25] T. Strassle, F. Juranyi, M. Schneider, S. Janssen, A. Furrer, K. W. Kramer, and H. U. Güdel, Phys. Rev. Lett. **92**257202 (2004).
[26] B. P. Alho, N. A. de Oliveira, V. S. R. de Sousa, S. Gama, A. A. Coelho, A. M. G. Carvalho, and P. J. von Ranke, Solid State Commun. **152**, 951 (2012).
[27] N. A. de Oliveira, P. J. von Ranke, and A. Troper, Int. J. Refrig. **37**, 237 (2014).
[28] R. P. Santana, N. A. de Oliveira, and P. J. von Ranke, J. Phys.: Condens. Matter. **23**, 306003 (2011).
[29] J. S. Dugdale and D. K. C. MacDonald, Phys. Rev. **89**, 832 (1953).
[30] E. Grüneisen, Ann. Phys. **344**, 257 (1912).
[31] C. P. Bean and D. S. Rodbell, Phys. Rev. **126**, 104 (1962).
[32] O. Svitelskiy, A. Suslov, D. L. Schlagel, T. A. Lograsso, K. A. Gschneidner Jr., and V. K. Pecharsky, Phys. Rev. B **74**, 184105 (2006).
[33] T. S. T. Alvarenga, B. P. Alho, E. P. Nóbrega, P. O. Ribeiro, A. Caldas, V. S. R. de Sousa, A. M. G. Carvalho, N. A. de Oliveira, and P. J. von Ranke, J. Appl. Phys. **116**, 243908 (2014).
[34] P. J. von Ranke, N. A. de Oliveira, C. Mello, A. M. G. Carvalho, and S. Gama, Phys. Rev. B **71**, 054410 (2005).
[35] K. Binder, Rep. Prog. Phys. **50**, 783 (1987).
[36] J. Langer, Physica **73**, 61 (1974).
[37] S. Valadkhan, K. Morris, and A. Khajepour, J. Intell. Mater. Syst. Struct. **20**131 (2009).
[38] G. Berlotti, *Hysteresis in Magnetism: For Physicists, Materials Scientists and Engineers* (Academic Press, San Diego, CA, 1998).
[39] N. A. de Oliveira and P. J. von Ranke, Phys. Rep. **489**, 89 (2010).
[40] P. Kumar, K. G. Suresh, and A. K. Nigam, J. Phys. D: Appl. Phys. **41**, 105007 (2008).
[41] V. K. Pecharsky, K. A. Gschneidner Jr., A. O. Pecharsky, and A. M. Tishin, Phys. Rev. B **64**, 144406 (2001).